



## Semi-active links in double-panel noise barriers

Stanislaw Wrona<sup>a,\*</sup>, Marek Pawelczyk<sup>a</sup>, Li Cheng<sup>b</sup>

<sup>a</sup> Silesian University of Technology, Department of Measurements and Control Systems, Gliwice, Poland

<sup>b</sup> Department of Mechanical Engineering, Hong Kong Polytechnic University, Hong Kong, China



### ARTICLE INFO

#### Article history:

Received 15 June 2020

Received in revised form 8 November 2020

Accepted 8 December 2020

#### Keywords:

Mathematical modelling

Acoustic radiation

Double wall

Vibrating plates

Semi-active control

### ABSTRACT

Active control methods have shown their effectiveness in reducing noise transmitted through single- or double-panel barriers. However, when the availability of high-performance processors and energy sources is limited, it is worth considering alternative solutions, including semi-active methods. They can offer considerable levels of noise reduction with limited resources and lower application costs. This paper investigates a novel semi-active control approach for double-panel noise barriers, where bistable links mounted between the panels are structurally coupled, when turned on, or decoupled, when turned off. These semi-active links only require energy when switching between states. The structural couplings significantly alter natural frequencies and mode shapes of the vibroacoustic system. This enables an adaptation of structural response dependent on the noise spectrum, i.e. minimizing the radiation in the targeted frequency bands. Such an approach is especially feasible in case of non-stationary narrow-band noise, which is very common in real-life. Analysis of experimental results shows that the acoustic radiation of a noise barrier can be reduced by as much as 16 dB for targeted resonance frequencies.

© 2020 Elsevier Ltd. All rights reserved.

## 1. Introduction

People are often exposed to excessive acoustic noise in modern society and as a result, a variety of noise reduction methods have been developed. One such approach is to separate the recipients from the noise source using noise barriers. Commonly used passive barriers are generally ineffective for low-frequency noise. They also tend to be thick and heavy and introduce unwanted heat insulation. However, thanks to technological advancement, passive barriers can be complemented with or replaced by actively controlled barriers. They incorporate control sources that may be either acoustic, such as loudspeakers, or structural, such as vibration actuators. Such systems are most effective in the low-frequency range, where passive insulation fails. Actively controlled barriers have proven their effectiveness in a number of publications. Milton et al. implemented active structural acoustic control of a rectangular plate using an experimentally identified radiation resistance matrix [1]. Wrona et al. achieved an active reduction of a device narrowband noise by controlling vibration of a whole custom-made cubic casing [2]. Mazur et al. actively reduced washing machine noise by controlling vibrations of its original ready-made casing [3]. Li et al. analysed an active control of sound transmitted through a linked double-wall system into an acoustic cavity [4]. In some applications, openings with dedicated active noise control systems can also be integrated into barriers to allow natural ventilation and light, as presented by Qiu in [5] or by Shi et al. in [6]. However, when the availability

\* Corresponding author.

E-mail addresses: [stanislaw.wrona@polsl.pl](mailto:stanislaw.wrona@polsl.pl) (S. Wrona), [marek.pawelczyk@polsl.pl](mailto:marek.pawelczyk@polsl.pl) (M. Pawelczyk), [li.cheng@polyu.edu.hk](mailto:li.cheng@polyu.edu.hk) (L. Cheng).

## Nomenclature

### Symbols

$c_p$	sound speed in the air
$D_a$	flexural rigidity of the panel $a$
$E_a$	Young's modulus of the panel $a$
$f_{L,j}$	force produced by the $j$ th link
$h_a$	thickness of the panel $a$
$H_{ij}$	coefficients of the coupled system
$k_e$	acoustic wavenumber
$K_{L,j}$	stiffness of $j$ th semi-active link
$\mathbf{K}_a$	stiffness matrix
$L_{a,x}, L_{a,y}$	dimensions of the panel $a$
$L_{b,x}, L_{b,y}$	dimensions of the panel $b$
$L_{e,x}, L_{e,y}, L_{e,z}$	dimensions of the enclosure
$L_{g,x}, L_{g,y}, L_{g,z}$	dimensions of the gap cavity
$L_{ae,ij}, L_{ag,ij}, L_{bg,ij}$	modal coupling coefficients
$m_{a,i}, m_{b,i}, m_{e,i}, m_{g,i}$	generalized modal mass of the $i$ th mode
$m_{La,i}, m_{Lb,i}$	masses of the $i$ th link components attached to panel $a$ and $b$ , respectively
$\mathbf{M}_a$	mass matrix
$N_a, N_b, N_e, N_g$	numbers of modes considered for panels $a$ and $b$ , the enclosure and the gap cavity, respectively
$N_L$	number of links
$p_{e,i}, p_{g,i}$	$i$ th modal pressure amplitude of the enclosure and the gap cavity, respectively
$P_e, P_g$	acoustic pressures inside the enclosure and the gap cavity, respectively
$p_{ext,i}(x,y,z)$	external modal acoustic pressure amplitude corresponding to $i$ th mode of the system
$P_{ext,i}$	external modal acoustic power corresponding to $i$ th mode of the system
$\mathbf{q}_a$	generalized panel $a$ displacement vector
$S_a, S_b$	surfaces of panels $a$ and $b$ , respectively
$S_{ext}$	surface enclosing the barrier
$t$	time
$T_a, T_{a,w}, T_{aL}$	overall kinetic energy, kinetic energy of the panel and kinetic energy of the links, respectively
$U_a, U_{a,w}$	overall potential energy and potential energy of the panel, respectively
$\mathbf{v}_a, \mathbf{v}_b$	modal displacement vectors
$V_e, V_g$	volume of the enclosure and the gap cavity, respectively
$w_a, w_b$	displacement of panels $a$ and $b$ , respectively
$i, j, k$	positive integers
$x, y, z$	coordinates
$x_{L,i}, y_{L,i}$	coordinates of the $i$ th link
$l$	imaginary number
$\nu_a$	Poisson ratio of the panel $a$
$\xi_{a,i}, \xi_{b,i}, \xi_{e,i}, \xi_{g,i}$	damping coefficients
$\rho_a$	mass density of the panel $a$ material
$\rho_p$	equilibrium air density
$\Phi_a$	vector of trial functions
$\psi_{a,i}, \psi_{b,i}$	mode shapes of the loaded panels $a$ and $b$ , respectively
$\psi_{e,i}, \psi_{g,i}$	mode shapes of the enclosure and the gap cavity, respectively
$\Phi_a$	eigenvector matrix
$\omega_{a,i}, \omega_{b,i}$	$i$ th eigenfrequencies of uncoupled panels $a$ and $b$ , respectively
$\omega_{e,i}, \omega_{g,i}$	$i$ th eigenfrequencies of uncoupled enclosure and gap cavity, respectively
$\omega_{c,i}$	$i$ th coupled natural angular frequency of the system
$\Omega_a$	eigenfrequencies matrix
$\xi, \eta, \gamma$	components of the acoustic wavevector

of high-performance processors and energy sources is limited, it can be beneficial to adopt a semi-active solution instead. The semi-active barrier adjusts the characteristics of the structure itself with a small external energy supply [7]. It can offer considerable levels of noise reduction in a highly effective and economical manner.

Double-panel structures can be used as a base on which to design semi-active noise barriers. Double-wall structures have been widely used in aircraft fuselages, car doors and lightweight partition walls in buildings because they offer significantly higher passive transmission loss compared to equivalent single-wall structures. However, their acoustic performance deteriorates rapidly at low frequencies due to low order structural-acoustic resonances. So called mass-air-mass resonance is particularly responsible for the weak passive transmission loss [8,9]. This is the frequency range where control systems can offer significant enhancement. This topic has gained a high interest in recent years. Langfeldt et al. considered a broadband low-frequency sound transmission loss improvement of double walls due to application of Helmholtz resonators [10]. De Melo Filho et al. studied dynamic mass based sound transmission loss prediction of vibro-acoustic metamaterial double panels applied to the mass-air-mass resonance [11]. Mao investigated an improvement on sound transmission loss through a double-plate structure by using electromagnetic shunt damper [12]. Ma et al. analyzed an active control of sound transmission through orthogonally rib stiffened double-panel structure [13]. In addition, double-panel structures enable application of a wide variety of control approaches, including (i) methods aimed at reduction of panel vibrations to reduce the acoustic radiation, and (ii) methods aimed at reduction of the acoustic response in the gap cavity to block the sound transmission. The first group consists of, e.g. tunable vibration absorbers [14] and piezoelectric patches with shunt circuits. Gardonio et al. investigated a panel with self-tuning shunted piezoelectric patches for broadband flexural vibration control [15]. Billon et al. studied vibration isolation and damping using a piezoelectric flexensional suspension with a negative capacitance shunt [16]. Dal Bo et al. considered a smart panel with sweeping and switching piezoelectric patch vibration absorbers [17]. On the other hand, the second group includes, e.g. adaptive Helmholtz resonators [10,18] and shunted loudspeakers located in the gap cavity between the panels [19].

This paper investigates a novel semi-active approach for double-panel noise barriers. The proposed solution can significantly enhance the effective transmission loss, while being significantly lighter and requiring less space compared to vibration absorbers or Helmholtz resonators (which can be bulky when tuned for low frequencies). Meanwhile, it is less demanding in terms of system complexity as compared with a fully active approach. The solution is based on bistable links mounted between the incident and the radiating panels, which structurally couple (when turned on) or decouple (when turned off). Such semi-active links only require energy for switching between the states. They do not force vibration by themselves and hence the solution is semi-active. The structural couplings that have been introduced significantly alter the natural frequencies and mode shapes of the vibroacoustic system. This enables an adaptation of frequency-dependent transmission loss to the noise spectrum, which can be easily monitored, i.e. minimizing the radiation in the targeted frequency bands (especially in the vicinity of low-order resonances). Such an approach aims at an efficient reduction of transmission of non-stationary narrow-band noise, which is very common in real-life.

This paper is organized as follows. Section 2 introduces a mathematical model of the double-panel barrier, including semi-active point links, loading due to their mass, and adjacent enclosure for the noise source. Section 3 discusses the results of an experimental validation of the model and the semi-active control approach designed by the authors. Section 4 presents the numerical simulation studies based on the validated model, providing analysis and insight into various practical aspects, including analysis of the energy transmission process. Section 5 summarizes the obtained results and conclusions.

## 2. Model of the vibroacoustic system

The vibroacoustic system considered in this paper is presented in Fig. 1. It can be divided into four explicitly modeled subsystems: two cavities and two thin panels. The first cavity is the enclosure, where a noise source is placed. The generated

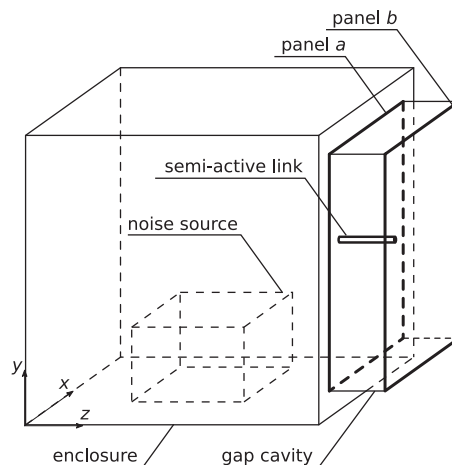


Fig. 1. A schematic representation of the vibroacoustic system.

noise excites the incident panel  $a$ , which through the gap cavity transmits the energy further to panel  $b$ . Panel  $b$  radiates the noise to the external environment. Energy from panel  $a$  to panel  $b$ , apart from the acoustic path through the air gap, can be transmitted through semi-active links, which, when turned on, structurally couple the panels. In addition, apart from the two panels  $a$  and  $b$ , in the reported research all other surfaces surrounding both the enclosure and the gap cavity are acoustically rigid.

To model the system under consideration, firstly all subsystems are described individually in order to obtain their natural frequencies and mode shapes. Then, interactions between the subsystems are introduced and a coupled system description is formed. Finally, the acoustic radiation of the whole barrier is estimated.

## 2.1. Models of the individual subsystems

### 2.1.1. Model of vibrating plates

For an isotropic and homogeneous panel  $a$ , free vibrations are governed by a differential equation [20]:

$$D_a \nabla^4 w_a + \rho_a h_a \ddot{w}_a = 0, \quad (1)$$

where  $w_a(x, y, t)$  denotes the displacement of the panel  $a$  from the reference state in the  $z$ -direction,  $D_a = E_a h_a^3 / [12(1 - \nu_a^2)]$  is the flexural rigidity,  $E_a$  is Young's modulus,  $\nu_a$  is Poisson ratio,  $\rho_a$  is the mass density of the panel material,  $h_a$  is the panel thickness, and a superimposed dot stands for the time derivative.

Considering only the transverse motion and neglecting the effect of rotary inertia, the kinetic and strain energies of the panel  $a$ ,  $T_{a,w}$  and  $U_{a,w}$ , can be written as:

$$T_{a,w} = \frac{\rho_a h_a}{2} \iint_{S_a} \dot{w}_a^2 dx dy, \quad (2a)$$

$$U_{a,w} = \frac{D_a}{2} \iint_{S_a} \left\{ \left( \frac{\partial^2 w_a}{\partial x^2} \right)^2 + \left( \frac{\partial^2 w_a}{\partial y^2} \right)^2 + 2\nu_a \frac{\partial^2 w_a}{\partial x^2} \frac{\partial^2 w_a}{\partial y^2} + 2(1 - \nu_a) \left( \frac{\partial^2 w_a}{\partial x \partial y} \right)^2 \right\} dx dy, \quad (2b)$$

where  $S_a$  is the surface of the panel.

To reflect the fact that mounting of the panels is often imperfect (neither simply-supported nor fully-clamped), boundary conditions elastically restrained against rotation are adopted. They are represented by rotational springs distributed linearly along panel edges and defined by a uniform spring constant  $k_{a,b}$ . Classical boundary conditions of the plate can be obtained as limiting cases when the spring constant  $k_{a,b}$  approach its natural limits of zero or infinity, leading to simply-supported or fully-clamped boundary conditions, respectively. The strain energy stored in rotational springs,  $U_{a,b}$ , is given by:

$$U_{a,b} = \frac{k_{a,b}}{2} \left[ \int_0^{L_{a,y}} \left\{ \left( \frac{\partial w_a}{\partial x} \right)^2 \Big|_{x=0} + \left( \frac{\partial w_a}{\partial x} \right)^2 \Big|_{x=L_{a,x}} \right\} dy + \int_0^{L_{a,x}} \left\{ \left( \frac{\partial w_a}{\partial y} \right)^2 \Big|_{y=0} + \left( \frac{\partial w_a}{\partial y} \right)^2 \Big|_{y=L_{a,y}} \right\} dx \right]. \quad (3)$$

Semi-active links considered in this research, apart from panel coupling, also load the panels with their mass, even if they are turned off. This loading affects the natural frequencies and mode shapes, and therefore it should be included in the model of the panel subsystem. The loading is represented by the additional concentrated mass attached to the panel surface. The effect of strain caused by the bonding of links to the plate surface is neglected. Thus, the total energy introduced to the system is considered to be the kinetic energy which is expressed as:

$$T_{a,L} = \sum_{i=1}^{N_L} \frac{m_{La,i}}{2} \dot{w}(x_{L,i}, y_{L,i})^2, \quad (4)$$

where  $N_L$ ,  $m_{La,i}$ ,  $x_{L,i}$  and  $y_{L,i}$  are the number of links, mass of the  $i$ th link component attached to panel  $a$ , and coordinates of the  $i$ th link, respectively.

The Rayleigh-Ritz method is used to calculate an approximate solution of the considered differential equation, obtaining panel natural frequencies and mode shapes [21]. To use this method the total energy of the system and trial functions needs to be defined. The energy functionals have already been derived in Eqs. (2)–(4), while characteristic orthogonal polynomials, with the property of Euler-Bernoulli beam functions, are used as the trial functions [22]. For free vibration of the considered panel, the solution of  $w_a$  can be expressed in the required form using a predetermined set of admissible trial functions:

$$w_a(x, y, t) = \sum_{i=1}^{N_a} \phi_{a,i}(x, y) q_{a,i}(t) = \boldsymbol{\phi}_a^T \mathbf{q}_a, \quad (5)$$

where  $\mathbf{q}_a$  is a generalized panel  $a$  displacement vector,  $\boldsymbol{\phi}_a$  is a vector which represents a set of time-invariant trial functions  $\phi_{a,i}(x, y)$ , and the superscript T denotes the transpose. All of these vectors have dimensions  $(N_a \times 1)$ , where  $N_a$  is the number of trial functions used.

Utilizing Eq. (5), the total kinetic and potential energies of panel  $a$ ,  $T_a = T_{a,w} + T_{a,L}$  and  $U_a = U_{a,w} + U_{a,b}$ , can also be written as functions of the generalized plate displacement vector  $\mathbf{q}_a$ , the mass matrix  $\mathbf{M}_a$  of dimensions  $(N_a \times N_a)$  and the stiffness matrix  $\mathbf{K}_a$  of dimensions  $(N_a \times N_a)$  as follows:

$$T_a = \frac{1}{2} \dot{\mathbf{q}}_a^T \mathbf{M}_a \dot{\mathbf{q}}_a, \quad U_a = \frac{1}{2} \mathbf{q}_a^T \mathbf{K}_a \mathbf{q}_a. \quad (6)$$

The elements of the mass matrix  $\mathbf{M}_a$  and stiffness matrix  $\mathbf{K}_a$ , respectively, are defined as:

$$M_{a,ij} = \rho_a h_a \iint_{S_a} \phi_{a,i} \phi_{a,j} dx dy + \sum_{k=1}^{N_L} m_{L,a,k} \phi_{a,i}(x_{L,k}, y_{L,k}) \phi_{a,j}(x_{L,k}, y_{L,k}), \quad (7a)$$

$$K_{a,ij} = D_a \iint_{S_a} \left\{ \frac{\partial^2 \phi_{a,i}}{\partial x^2} \frac{\partial^2 \phi_{a,j}}{\partial x^2} + \frac{\partial^2 \phi_{a,i}}{\partial y^2} \frac{\partial^2 \phi_{a,j}}{\partial y^2} + 2\nu_a \frac{\partial^2 \phi_{a,i}}{\partial x^2} \frac{\partial^2 \phi_{a,j}}{\partial y^2} + 2(1 - \nu_a) \frac{\partial^2 \phi_{a,i}}{\partial x \partial y} \frac{\partial^2 \phi_{a,j}}{\partial x \partial y} \right\} dx dy \\ + k_{a,b} \left[ \int_0^{L_{a,y}} \left\{ \left( \frac{\partial \phi_{a,i}}{\partial x} \frac{\partial \phi_{a,j}}{\partial x} \right) \Big|_{x=0} + \left( \frac{\partial \phi_{a,i}}{\partial x} \frac{\partial \phi_{a,j}}{\partial x} \right) \Big|_{x=L_{a,x}} \right\} dy \right. \\ \left. + \int_0^{L_{a,x}} \left\{ \left( \frac{\partial \phi_{a,i}}{\partial y} \frac{\partial \phi_{a,j}}{\partial y} \right) \Big|_{y=0} + \left( \frac{\partial \phi_{a,i}}{\partial y} \frac{\partial \phi_{a,j}}{\partial y} \right) \Big|_{y=L_{a,y}} \right\} dx \right]. \quad (7b)$$

Having defined the stiffness and mass matrices by using the Lagrange equation of the second kind the equation of a vibrating structure can be obtained as:

$$\mathbf{M}_a \ddot{\mathbf{q}}_a + \mathbf{K}_a \mathbf{q}_a = \mathbf{0}, \quad (8)$$

The harmonic solution to Eq. (8) gives the eigenvector matrix  $\Phi_a$  with dimensions  $(N_a \times N_a)$  and  $N_a$  eigenfrequencies  $\omega_{a,i}$ . Replacing  $\mathbf{q}_a^T$  by  $\Phi_a \mathbf{v}_a$  and multiplying Eq. (8) on the left by  $\Phi_a^T$  gives:

$$\Phi_a^T \mathbf{M}_a \Phi_a \ddot{\mathbf{v}}_a + \Phi_a^T \mathbf{K}_a \Phi_a \mathbf{v}_a = \mathbf{0}, \quad (9)$$

where  $\mathbf{v}_a$  denotes the modal displacement vector of dimensions  $(N_a \times 1)$ . Taking advantage of the orthonormality of the eigenvectors in matrix  $\Phi_a$ , the modal mass matrix becomes a unit matrix  $\mathbf{I}_{N_a}$  of dimensions  $(N_a \times N_a)$  and the corresponding modal stiffness matrix becomes a diagonal matrix  $\Omega_a$  of  $N_a$  eigenvalues  $\omega_{a,i}^2$  [23], which gives:

$$\Phi_a^T \mathbf{M}_a \Phi_a = \mathbf{I}_{N_a}, \quad \Phi_a^T \mathbf{K}_a \Phi_a = \Omega_a = \left[ \text{diag}(\omega_{a,1}^2, \omega_{a,2}^2, \dots, \omega_{a,N_a}^2) \right]. \quad (10)$$

Then, substituting Eq. (10) into Eq. (9), gives:

$$\ddot{\mathbf{v}}_a + \Omega_a \mathbf{v}_a = \mathbf{0}, \quad (11)$$

with

$$w_a(x, y, t) = \sum_{i=1}^{N_a} \left( \sum_{j=1}^{N_a} \Phi_{a,ji} \phi_{a,i}(x, y) \right) v_{a,i}(t) = (\Phi_a^T \phi_a)^T \mathbf{v}_a = \Psi_a^T \mathbf{v}_a, \quad (12a)$$

where  $\Psi_a$  represents a vector of mode shapes of the loaded panel  $a$ . Introducing a modal loss factor  $\zeta_{a,i}$ , and interactions with enclosure, gap cavities and panel  $b$  to Eq. (11), a set of ordinary differential equations can be written:

$$\dot{v}_{a,i} + 2\zeta_{a,i} \omega_{a,i} v_{a,i} + \omega_{a,i}^2 v_{a,i} = \frac{1}{m_{a,i}} \left[ \iint_{S_a} (P_e - P_g) \psi_{a,i} dx dy - \sum_{j=1}^{N_L} f_{L,j} \psi_{a,i}(x_{L,j}, y_{L,j}) \right], \quad (13a)$$

where  $P_e$  and  $P_g$  are the acoustic pressures inside the enclosure and the gap cavity respectively,  $m_{a,i}$  is the generalized modal mass of the  $i$ th mode, and  $f_{L,j}$  is the force produced by the  $j$ th semi-active link located at  $(x_{L,j}, y_{L,j})$  coordinates, which, when turned on, can be simulated by a spring with a stiffness  $K_{L,j}$  as:

$$f_{L,j} = K_{L,j} \left( \sum_{i=1}^{N_a} \psi_{a,i}(x_{L,j}, y_{L,j}) v_{a,i}(t) - \sum_{i=1}^{N_b} \psi_{b,i}(x_{L,j}, y_{L,j}) v_{b,i}(t) \right). \quad (13b)$$

Similarly, the displacement of the panel  $b$ ,  $w_b(x, y, t)$ , can be expressed as:

$$\dot{v}_{b,i} + 2\zeta_{b,i} \omega_{b,i} v_{b,i} + \omega_{b,i}^2 v_{b,i} = \frac{1}{m_{b,i}} \left[ \iint_{S_b} P_g \psi_{b,i} dx dy + \sum_{j=1}^{N_L} f_{L,j} \psi_{b,i}(x_{L,j}, y_{L,j}) \right], \quad (13c)$$

where quantities with the subscript "b" have the same meaning as those defined before, but apply to panel  $b$ . The acoustic pressure loading from the exterior on the radiating panel  $b$  is neglected.

2.1.2. Model of acoustic pressure inside the cavities

The acoustic pressures inside the enclosure,  $P_e$ , is governed by the classical wave equation [24]:

$$\nabla^2 P_e - \frac{1}{c_p^2} \frac{\partial^2 P_e}{\partial t^2} = 0, \tag{14}$$

where  $c_p$  is the speed of sound in the air. Possible sources and interactions with panels would be on the right hand side, however, for the moment the sole subsystem is considered. Assuming the enclosure as a closed rectangular volume with hard boundary surface, the natural angular frequencies and mode shapes,  $\omega_{e,ijk}$  and  $\psi_{e,ijk}$ , respectively, can be calculated with closed-form formulae: [24]

$$\omega_{e,ijk} = c_p \pi \left( \frac{i^2}{L_{e,x}^2} + \frac{j^2}{L_{e,y}^2} + \frac{k^2}{L_{e,z}^2} \right)^{1/2}, \tag{15a}$$

$$\psi_{e,ijk} = \cos \frac{i\pi x}{L_{e,x}} \cos \frac{j\pi y}{L_{e,y}} \cos \frac{k\pi z}{L_{e,z}}, \tag{15b}$$

$$i, j, k = 0, 1, 2, \dots,$$

where  $L_{e,x}$ ,  $L_{e,y}$ , and  $L_{e,z}$  are the dimensions of the enclosure in the  $x, y$  and  $z$  directions, respectively. Sorting corresponding  $\omega_{e,ijk}$  and  $\psi_{e,ijk}$  by natural frequencies in ascending order, the triple subscript  $ijk$  can be reduced to single subscript  $i$ , obtaining  $\omega_{e,i}$  and  $\psi_{e,i}$  respectively. The acoustic modes are orthogonal over the enclosure volume  $V_e$  such that:

$$\frac{1}{V_e} \int_{V_e} \psi_{e,i} \psi_{e,j} dv = \begin{cases} 0, & i \neq j, \\ m_{e,i}, & i = j, \end{cases} \tag{16}$$

where  $V_e = L_{e,x}L_{e,y}L_{e,z}$ , and  $m_{e,i}$  is the  $i$ th modal generalized mass of the enclosure. Based on mode shapes that were obtained,  $P_e$  can be decomposed as:

$$P_e(x, y, z, t) = \sum_{i=1}^{N_e} \psi_{e,i}(x, y, z) p_{e,i}(t) = \boldsymbol{\psi}_e^T \mathbf{p}_e, \tag{17}$$

where  $p_{e,i}$  is the  $i$ th modal pressure amplitude of the enclosure, and  $N_e$  is the number of modes included in the decomposition.

Employing a transformation given in [25], and introducing a modal loss factor  $\zeta_{e,i}$  and interaction with panel  $a$ , the wave equation can be transformed into a set of ordinary differential equations, obtaining:

$$\ddot{p}_{e,i} + 2\zeta_{e,i}\omega_{e,i}\dot{p}_{e,i} + \omega_{e,i}^2 p_{e,i} = \frac{\rho_p c_p^2}{m_{e,i} V_e} \left[ - \iint_{S_a} \ddot{w}_a \psi_{e,i} dx dy \right], \tag{18a}$$

where  $\rho_p$  is the equilibrium air density. Similarly, the acoustic pressure  $P_g$  inside the gap cavity can be expressed as:

$$\ddot{p}_{g,i} + 2\zeta_{g,i}\omega_{g,i}\dot{p}_{g,i} + \omega_{g,i}^2 p_{g,i} = \frac{\rho_p c_p^2}{m_{g,i} V_g} \left[ \iint_{S_a} \ddot{w}_a \psi_{g,i} dx dy - \iint_{S_b} \ddot{w}_b \psi_{g,i} dx dy \right], \tag{18b}$$

where quantities with the subscript ‘‘g’’ have the same meaning as those defined before but apply to the gap cavity.

2.2. Coupling of subsystems

Using the approach presented in [25], description of individual subsystems given in Eqs. (12) and (18) can be combined together forming a set of ordinary differential equations:

$$\ddot{v}_{a,i} + 2\zeta_{a,i}\omega_{a,i}\dot{v}_{a,i} + \omega_{a,i}^2 v_{a,i} = \frac{1}{m_{a,i}} \left[ S_a \left( \sum_{j=1}^{N_e} L_{ae,ij} p_{e,j} - \sum_{j=1}^{N_g} L_{ag,ij} p_{g,j} \right) - \sum_{j=1}^{N_l} f_{Lj} \psi_{a,i}(x_{Lj}, y_{Lj}) \right], \tag{19a}$$

$$\ddot{v}_{b,i} + 2\zeta_{b,i}\omega_{b,i}\dot{v}_{b,i} + \omega_{b,i}^2 v_{b,i} = \frac{1}{m_{b,i}} \left[ S_b \sum_{j=1}^{N_g} L_{bg,ij} p_{g,j} + \sum_{j=1}^{N_l} f_{Lj} \psi_{b,i}(x_{Lj}, y_{Lj}) \right], \tag{19b}$$

$$\ddot{p}_{e,i} + 2\zeta_{e,i}\omega_{e,i}\dot{p}_{e,i} + \omega_{e,i}^2 p_{e,i} = \frac{\rho_p c_p^2}{m_{e,i} V_e} \left[ -S_a \sum_{j=1}^{N_a} L_{ae,ji} \dot{v}_{a,j} \right], \tag{19c}$$

$$\ddot{p}_{g,i} + 2\zeta_{g,i}\omega_{g,i}\dot{p}_{g,i} + \omega_{g,i}^2 p_{g,i} = \frac{\rho_p c_p^2}{m_{g,i} V_g} \left[ S_a \sum_{j=1}^{N_a} L_{ag,ji} \dot{v}_{a,j} - S_b \sum_{j=1}^{N_b} L_{bg,ij} \dot{v}_{b,j} \right], \tag{19d}$$

where  $L_{ae,ij}$ ,  $L_{ag,ij}$  and  $L_{bg,ij}$  are modal coupling coefficients between the  $i$ th structural mode of panel  $a$  (or  $b$ ) and  $j$ th cavity mode of the enclosure (or the gap cavity), respectively:

$$L_{ae,ij} = \frac{1}{S_a} \int_{S_a} \psi_{a,i} \psi_{e,i} dx dy, \quad L_{ag,ij} = \frac{1}{S_a} \int_{S_a} \psi_{a,i} \psi_{g,i} dx dy, \quad L_{bg,ij} = \frac{1}{S_b} \int_{S_b} \psi_{b,i} \psi_{g,i} dx dy. \tag{20}$$

In the case where the harmonic excitation is assumed:

$$v_{a,i}(t) = a_i e^{i\omega t}, \quad v_{b,i}(t) = b_i e^{i\omega t}, \quad p_{e,i}(t) = c_i e^{i\omega t}, \quad p_{g,i}(t) = d_i e^{i\omega t}, \tag{21}$$

Eqs. (19) can be written in a matrix form:

$$\begin{bmatrix} H_{11} & H_{12} & H_{13} & H_{14} \\ H_{21} & H_{22} & 0 & H_{24} \\ H_{31} & 0 & H_{33} & 0 \\ H_{41} & H_{42} & 0 & H_{44} \end{bmatrix} \begin{bmatrix} A \\ B \\ C \\ D \end{bmatrix} = \begin{bmatrix} 0 \\ 0 \\ F_e \\ 0 \end{bmatrix}, \tag{22}$$

where  $H_{ij}$  are coefficients defined in the Appendix A,  $F_e$  is generalized excitation applied to the enclosure cavity modes,  $A = [a_1, \dots, a_{N_a}]^T$ ,  $B = [b_1, \dots, b_{N_b}]^T$ ,  $C = [c_1, \dots, c_{N_e}]^T$ ,  $D = [d_1, \dots, d_{N_g}]^T$ , and  $i$  is the imaginary number satisfying equation  $i^2 = -1$ .

### 2.3. Acoustic radiation of the barrier

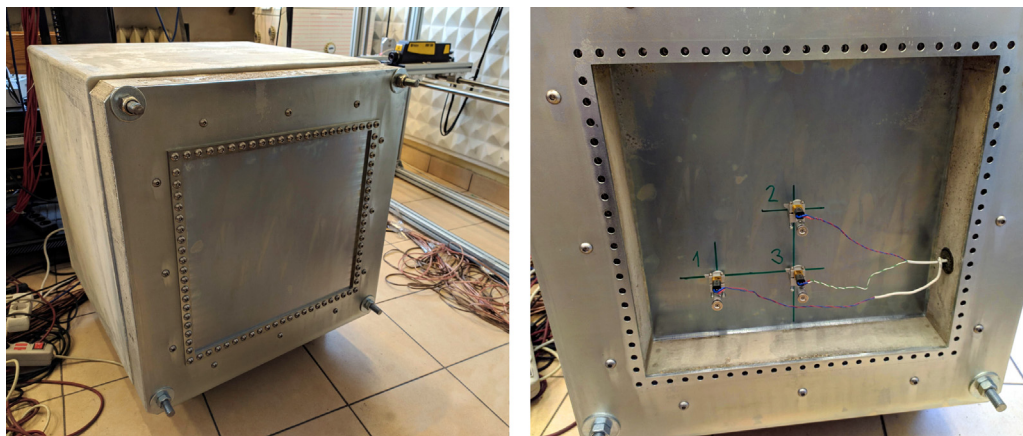
The aim of this subsection is to determine an estimate of the acoustic power radiated by the barrier corresponding to the  $i$ th coupled mode of the radiating panel  $b$ . To describe the acoustic radiation of the panel, it has been assumed that it is placed in an infinite rigid baffle. Adopting an appropriate Green's function that has been derived in [26,27], the modal sound pressure amplitude  $p_{ext,i}(x, y, z)$  can be calculated as:

$$p_{ext,i}(x, y, z) = \frac{k_e L_{b,x} L_{b,y}}{4\pi^2} \rho_p c_p \iint_{-\infty}^{+\infty} \exp [i(\xi x + \eta y + \gamma z)] M_i(\xi, \eta) \frac{d\xi d\eta}{\gamma}, \tag{23}$$

where:

$$M_i(\xi, \eta) = \frac{-2 i \omega_{c,i}}{L_{b,x} L_{b,y}} \iint_{S_p} \psi_{b',i} \exp [-i(\xi x + \eta y)] dx dy. \tag{24}$$

In Eqs. (23) and (24) the symbol  $k_e = \omega_{c,i}/c_p$  is the acoustic wavenumber,  $\xi, \eta$  and  $\gamma$  are the components of the acoustic wavevector,  $\omega_{c,i}$  is the  $i$ th coupled natural angular frequency of the structure, and  $\psi_{b',i}$  is the  $i$ th coupled mode shape of the panel  $b$ .



(a) A photograph of the heavy concrete box and mounted panel  $b$ . (b) A photograph with disassembled panel  $b$  and three semi-active links mounted in the gap cavity.

Fig. 2. Photographs of the laboratory setup.

To determine an estimate of the modal acoustic power,  $P_{ext,i}$ , the squared modal sound pressure under free-field conditions,  $p_{ext,i}(x, y, z)$ , can be averaged over a surface  $S_{ext}$ , which encloses the vibrating panel [28]. Hence, the modal acoustic power  $P_{ext,i}$  can be expressed as:

$$P_{ext,i} = \iint_{S_{ext}} \frac{|p_{ext,i}(x, y, z)|^2}{\rho_p c_p} dS_{ext}. \quad (25)$$

### 3. Experimental validation

This section presents results of an experimental validation of the mathematical model of a double-panel barrier. It also evaluates the designed semi-active actuators and the proposed approach to control. Photographs of the laboratory setup used for this purpose are shown in Fig. 2.

The enclosure was built as a heavily reinforced-concrete box, of which the walls can be considered as acoustically rigid. A loudspeaker was placed inside the enclosure as a noise source. For the purpose of model verification, the loudspeaker was driven to generate band-limited white noise. Two rectangular steel plates were attached to the front of the enclosure at a distance of  $L_{g,z} = 0.080$  m. The concrete walls of the box provided a high noise attenuation, hence most of the acoustic energy, which was transmitted outside the box, was transmitted through the panels. The dimensions of each panel area that was free to vibrate (i.e. the area inside the clamping frame) are  $0.420$  m  $\times$   $0.390$  m. The panels and cavities can be described by the following parameters (cf. Section 2 for the meaning of symbols):

the panels :

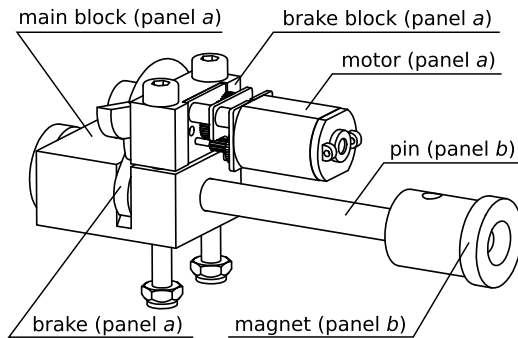
$$\begin{aligned} L_{a,x} = L_{b,x} &= 0.420 \text{ m}, & L_{a,y} = L_{b,y} &= 0.390 \text{ m}, & h_a = h_b &= 0.001 \text{ m}, \\ E_a = E_b &= 210 \text{ GPa}, & \rho_a = \rho_b &= 7850 \text{ kg/m}^3, & \nu_a = \nu_b &= 0.3, \\ k_{a,b} = k_{b,b} &= 340 \text{ N/rad}, & & & \zeta_{a,i} = \zeta_{b,i} &= 0.001, \end{aligned}$$

the cavities :

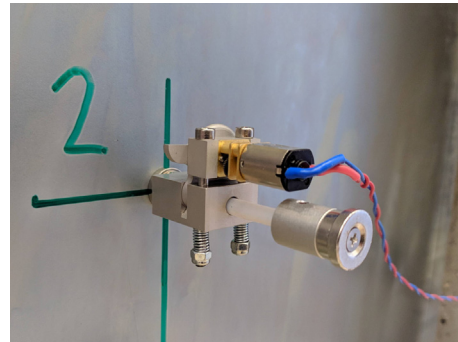
$$\begin{aligned} L_{e,x} &= 0.500 \text{ m}, & L_{e,y} &= 0.500 \text{ m}, & L_{e,z} &= 0.500 \text{ m}, \\ L_{g,x} &= 0.420 \text{ m}, & L_{g,y} &= 0.390 \text{ m}, & L_{g,z} &= 0.080 \text{ m}, \\ c_p &= 343 \text{ m/s}, & \rho_p &= 1.21 \text{ kg/m}^3, & \zeta_{e,i} = \zeta_{g,i} &= 0.001, \end{aligned}$$

A scheme and a photograph of the setup of the semi-active link are shown in Fig. 3. In Fig. 3a, each component described has the name of a panel to which it is attached denoted in parentheses, when the link is turned off (decoupled). The masses of  $i$ th semi-active link components are  $m_{La,i} = 0.043$  kg and  $m_{Lb,i} = 0.013$  kg. Both ends of the link are attached to the panels with neodymium magnets. To change the state of the link, the motor either rotates the brake counter-clockwise to hold the pin inside the main block (coupling panels) or rotates it clockwise to release the pin and allow it to move freely inside the main block. The motor only requires energy for a short time in order to switch between states, otherwise the system is self-locking. Pressure springs under the main block push the brake block down, ensuring that, when turned on, the brake holds the pin firmly. The pin is covered with a layer of PTFE to minimize friction when the link is turned off. Most of the components are made of stainless steel or aluminum, so the permanent magnets used for mounting the link to panels do not introduce additional forces acting on panels.

For validation, firstly the accuracy of modelling the panel vibration should be examined. For this purpose, the structural response of panel  $b$  was measured using a Polytec PDV-100 laser vibrometer mounted on an automatic positioning system developed by the authors. The positioning system allowed precise movement of the carriage with the vibrometer along both



(a) A scheme of the semi-active link.



(b) A photograph of the semi-active link.

Fig. 3. A scheme and a photograph of the setup of the semi-active link.

horizontal and vertical axes. Panel *a* was inaccessible for the non-contact measurements. The results obtained are compared with theoretical predictions in the following Section 3.1.

Secondly, the modeling of the acoustic radiation from the plate should be validated. For this purpose, two Beyerdynamic MM1 measurement microphones were mounted on the carriage along with the laser vibrometer. Although this validation has also been successfully done during this research work, for the sake of conciseness the verification data has been omitted in this paper because the acoustic radiation model has already been verified in [28] for a related scenario and the analogous verification data published. The acoustic radiation depends only on vibrations of panel *b*, thus it is analogous to a single-panel barrier considered in [28].

Finally, the experimental results of semi-active control are validated in 3.2 through a comparison of the double-panel barrier without the link and with a single optimally controlled semi-active link.

### 3.1. Verification of the modeling of panel vibrations

#### 3.1.1. Double-panel barrier without loading

This evaluation was carried out for a double-panel structure connected to an enclosure without any additional element attached to the surface of the panels. Theoretical results are compared with experimental measurements in Table 1. After a convergence study, the number of trial functions used for both panels was set to  $N_a = N_b = 256$  (the orthogonal polynomials were truncated at the order of 16 in both *x* and *y* direction). The orders of acoustic modes have been truncated at (8,8,8) for the enclosure and at (8,8,2) for the gap cavity. The mode shapes (or operational vibration shapes for measurements) are regular, hence  $\psi_{a,i}$  and  $\psi_{b,i}$  are described using a number of nodal lines minus one, parallel to the *y* and *x* direction, respectively (e.g. a fundamental mode of an unloaded rectangular plate has a mode shape denoted as (1,1)). Moreover, it has been assumed that panel *b* mode shapes are always positive, while panel *a* mode shapes can be both positive (vibrating in-phase with panel *b*) or negative (vibrating out-of-phase with panel *b*).

It follows from the analysis of Table 1 that the consistency between the results is high, both in terms of the natural frequencies and mode shapes. Nearly all of the initial 20 theoretically predicted modes could be distinguished with the laboratory setup. It clearly proves that the model of the double-panel structure is sufficiently accurate.

#### 3.1.2. Double-panel barrier with a coupling link between panels

The second evaluation was done for a double-panel structure with a semi-active link introduced between the panels at the center of the plates, at  $x_{L,1} = 0.5L_{a,x}$  and  $y_{L,j} = 0.5L_{a,y}$ . The link was turned on, coupling both panels together with stiffness of the link  $K_{L,1} = 10^6$  N/m. Such value represents a nearly completely stiff link and it has been estimated by trial and error method during preliminary tests.

Theoretical predictions are compared with experimental measurements in Table 2. The mode shape, or operational vibration shapes, are irregular in some cases, hence  $\psi_{a,i}$  and  $\psi_{b,i}$  are described either in the same manner as in the previous subsection or are depicted in Fig. 4. The consistency between the results, presented in Table 2, is again very good. Most of the initial 20 theoretically predicted modes could be distinguished with the laboratory setup. Again, the presented results prove

**Table 1**

Comparison of vibration simulations and measurements obtained for an unloaded double-panel structure. The symbol  $f_{c,i} = \omega_{c,i}/2\pi$  is the *i*th coupled natural frequency of the structure. Modal Assurance Criterion (MAC) [29] values are also given.

No.	Simulation			Experiment		MAC
	$f_{c,i}$	$\psi_{a,i}$	$\psi_{b,i}$	$f_{c,i}$	$\psi_{b,i}$	
1	54 Hz	+(1,1)	+(1,1)	48 Hz	+(1,1)	0.92
2	90 Hz	-(1,1)	+(1,1)	84 Hz	+(1,1)	0.91
3	100 Hz	-(2,1)	+(2,1)	102 Hz	+(2,1)	0.89
4	102 Hz	+(2,1)	+(2,1)	104 Hz	+(2,1)	0.81
5	109 Hz	-(1,2)	+(1,2)	115 Hz	+(1,2)	0.90
6	111 Hz	+(1,2)	+(1,2)	-	-	-
7	156 Hz	-(2,2)	+(2,2)	151 Hz	+(2,2)	0.88
8	157 Hz	+(2,2)	+(2,2)	162 Hz	+(2,2)	0.90
9	181 Hz	+(3,1)	+(3,1)	177 Hz	+(3,1)	0.83
10	184 Hz	-(3,1)	+(3,1)	188 Hz	+(3,1)	0.91
11	204 Hz	+(1,3)	+(1,3)	214 Hz	+(1,3)	0.88
12	208 Hz	-(1,3)	+(1,3)	-	-	-
13	233 Hz	-(3,2)	+(3,2)	231 Hz	+(3,2)	0.81
14	234 Hz	+(3,2)	+(3,2)	243 Hz	+(3,2)	0.87
15	246 Hz	-(2,3)	+(2,3)	246 Hz	+(2,3)	0.80
16	248 Hz	+(2,3)	+(2,3)	258 Hz	+(2,3)	0.84
17	285 Hz	-(4,1)	+(4,1)	285 Hz	+(4,1)	0.79
18	288 Hz	+(4,1)	+(4,1)	297 Hz	+(4,1)	0.81
19	322 Hz	-(1,4)	+(1,4)	323 Hz	+(1,4)	0.78
20	327 Hz	+(1,4)	+(1,4)	343 Hz	+(1,4)	0.77

**Table 2**  
Comparison of vibration simulations and measurements obtained for a double-panel structure with a link.

No.	Simulation			Experiment		MAC
	$f_{c,i}$	$\psi_{a',i}$	$\psi_{b',i}$	$f_{c,i}$	$\psi_{b',i}$	
1	51 Hz	+(1,1)	+(1,1)	45 Hz	+(1,1)	0.91
2	100 Hz	-(2,1)	+(2,1)	106 Hz	+(2,1)	0.88
3	102 Hz	+(2,1)	+(2,1)	-	-	-
4	109 Hz	-(1,2)	+(1,2)	117 Hz	+(1,2)	0.90
5	111 Hz	+(1,2)	+(1,2)	-	-	-
6	145 Hz	*	*	140 Hz	*	0.91
7	156 Hz	-(2,2)	+(2,2)	161 Hz	+(2,2)	0.89
8	158 Hz	+(2,2)	+(2,2)	-	-	-
9	171 Hz	+(3,1)	+(3,1)	172 Hz	+(3,1)	0.71
10	182 Hz	-(3,1)	+(3,1)	189 Hz	+(3,1)	0.83
11	192 Hz	*	*	203 Hz	*	0.84
12	198 Hz	+(1,3)	+(1,3)	-	-	-
13	230 Hz	-(3,2)	+(3,2)	241 Hz	+(3,2)	0.83
14	232 Hz	+(3,2)	+(3,2)	-	-	-
15	244 Hz	-(2,3)	+(2,3)	258 Hz	+(2,3)	0.86
16	246 Hz	+(2,3)	+(2,3)	-	-	-
17	271 Hz	*	*	277 Hz	*	0.86
18	278 Hz	+(4,1)	+(4,1)	-	-	-
19	309 Hz	+(3,3)	+(3,3)	317 Hz	+(3,3)	0.89
20	338 Hz	-(4,2)	+(4,2)	352 Hz	+(4,2)	0.83

\* Irregular mode shapes marked with a star are depicted in Fig. 4.

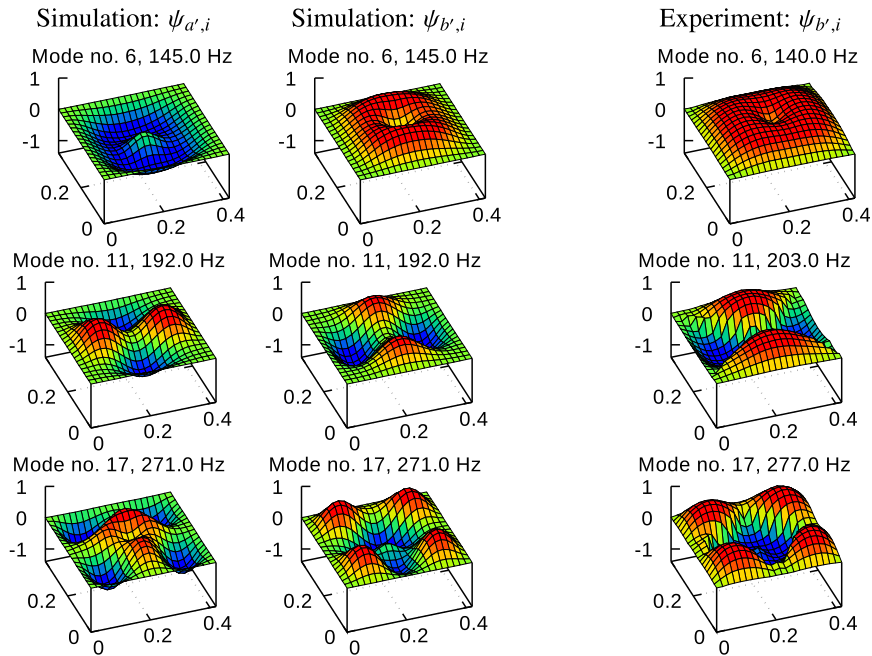


**Fig. 4.** A comparison between the theoretically calculated vibration mode shapes No. 6, 11 and 17 (irregularly shaped) with the corresponding experimentally measured operational vibration shapes.

that the derived model of the double-panel structure with semi-active links is accurate and can be used for simulation studies performed in the following section.

### 3.2. Verification of the semi-active control approach

Experimental results of the control system with the semi-active link are presented in this subsection. The mass-air-mass resonance, when both panels vibrate out-of-phase with mode shapes (1,1), is particularly responsible for noise transmission through double-panel barriers [30,11]. Hence, the semi-active link was attached to the centers of the panels to have the highest impact on the mass-air-mass resonance (its mode shape have the highest displacement of the panels at their centers). The

frequency characteristics of the mean vibration velocity of panel *b* and the mean squared external acoustic pressure are presented in Fig. 5. The adopted dB reference is equal to one, i.e. the frequency responses present the measured signal magnitude in the logarithmic scale without any additional normalization. However, to give a feeling about the experiments, the Sound Pressure Level of the noise in the room was between 75 and 85 dB. Vibration measurements of the panel were taken point-by-point with the vibrometer over a uniform grid of  $22 \times 20$  points, giving a total of 440 points, spaced at intervals of 0.02 m, hence covering the whole surface of panel *b*. After completing the measurements, the frequency analysis for all points was performed, and the mean vibration velocity was obtained by averaging all obtained frequency characteristics. The mean squared external acoustic pressure was calculated analogously by averaging frequency characteristics obtained with the microphones over the rectangular measurement grid, 1.00 m wide and 0.76 m high, 0.1 m away from the surface of panel *b*.

It follows from the analysis of Fig. 5ab that the activation of the link strongly alters the frequency response of the barrier. What is most noticeable, is that the aforementioned mass-air-mass resonance is relocated from 78 Hz to 140 Hz. It is very beneficial from the point of view of semi-active control. For example, to minimize the acoustic pressure due to noise transmitted through the barrier, the link should be turned on for tonal noise frequencies below 90 Hz, and turned off for frequencies between 90 Hz and 160 Hz (with some exceptions for narrow resonance peaks at 97 Hz and 100 Hz). Assuming that the noise is mainly tonal, although, it can be non-stationary, such action can reduce the mean acoustic pressure due to transmitted noise by even more than 16 dB. Thus, the objective is to protect the structure against excitation of the low-order structural-acoustic resonances, not to truly attenuate them (it would require much more energy). Shifting the resonances “away from the noise spectrum” in the frequency domain with semi-active elements is a much more efficient approach, as long as the noise is tonal or narrow-band, thus there are frequency bands where the resonances can be safely shifted to. Otherwise, for a broadband noise this approach would generally be not suitable, however, such cases are out of the scope of the proposed method.

The frequency characteristics for the “optimally controlled link” are presented in Figs. 5cd. The “optimally controlled link” means that the semi-active link is turned on or off, depending on which frequency characteristic is better for a given frequency (the minimum of both “on” and “off” characteristics is taken). The binary output controlling the link should be generated automatically by a controller. The controller is responsible to choose the more beneficial frequency response of the

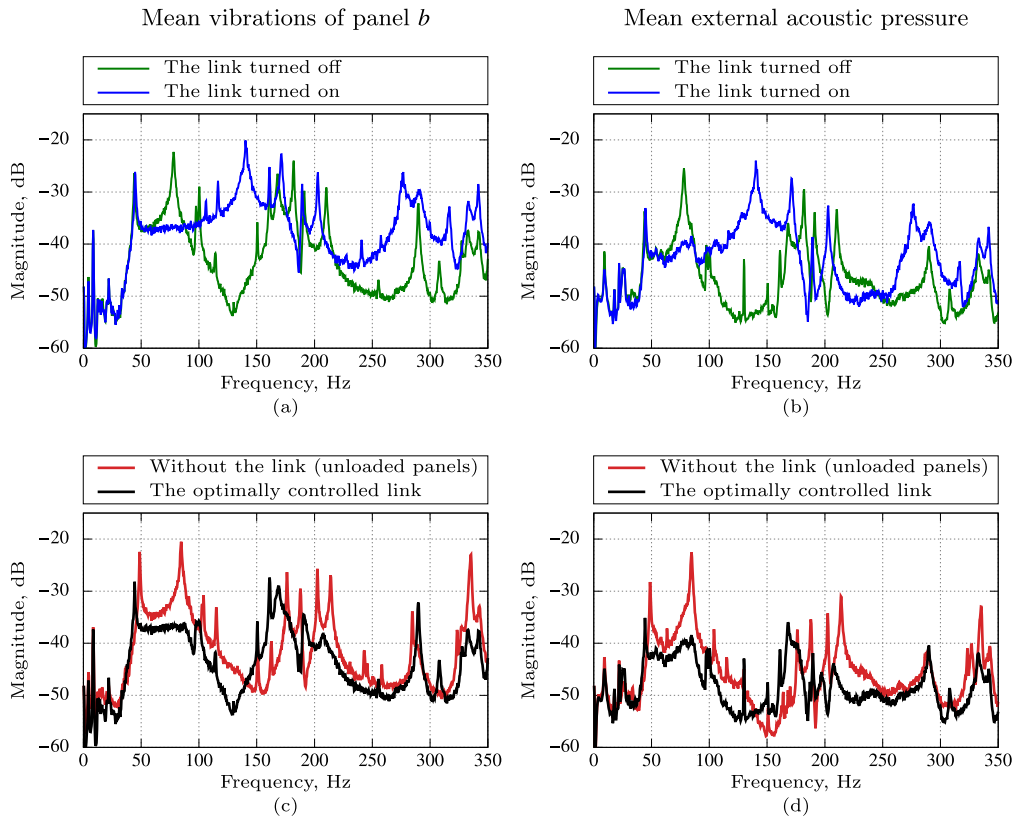


Fig. 5. Frequency characteristics for the semi-active control experiments performed for the link mounted between the panels at  $x_{L,1} = 0.5L_{a,x}$  and  $y_{L,j} = 0.5L_{a,y}$ . Plots (a) and (b) show a comparison of a double panel with the semi-active link turned off and on. Plots (c) and (d) show a comparison of a double panel without the link and with the optimally controlled semi-active link.

barrier according to a predefined cost function and the continuously monitored noise spectrum. The presented results assume a scenario where the noise is purely tonal. It is a simplification and the real noise might be more complex, however, it is assumed that in the targeted applications a single tone (or a narrow-band noise) is dominating the noise spectrum, thus the presented behaviour of avoidance of resonances excitation should be achievable in practice.

Obtained “optimal” characteristics are compared with a double-panel barrier without the link (unloaded panels) for a better evaluation of the provided performance. The total mass of the semi-active link is 0.056 kg, while both panels of the considered barrier weight 2.57 kg. The semi-active link increases the overall mass of the barrier by only approximately 2%. Hence, the mass of the link has a negligible impact on the noise reduction and the obtained noise reduction is a results of switching the link, hence choosing a more beneficial frequency response of the barrier for particular noise frequency.

It follows from the analysis that for most frequencies a barrier with just one semi-active link can provide better noise reduction of sound than the unloaded barrier without the link. Hence, it is worth exploring what performance could be achieved with other arrangements of panels and links. This concept is undertaken in the numerical simulation studies presented in the following section, basing on the already derived and validated mathematical model.

### 4. Simulation studies

#### 4.1. The semi-active link in the center of the panels

Firstly, a scenario already analyzed experimentally in Section 3.2 is once again considered using the simulation environment. The frequency characteristics obtained are presented in Fig. 6; the results are presented in an analogous manner as in Fig. 5. Both Figs. 5 and 6 are very consistent, especially regarding the main points, once again confirming the model accuracy (the overlaid characteristic are presented in Fig. 7). Firstly, the simulations presented also show that the semi-active link located in the center of the panels enables efficient mitigation of the mass-air-mass resonance originally located around 90 Hz (the excitation of the mass-air-mass resonance can be completely avoided due to switching of the semi-active link, what would not be possible with an addition of only a static mass). However, the fundamental mode (1,1) with panels vibrating in-phase is difficult to reduce in such a configuration when panels are of the same thickness. Moreover, the semi-active control enables the reduction of noise transmission for several other higher resonances. Some bands are slightly enhanced

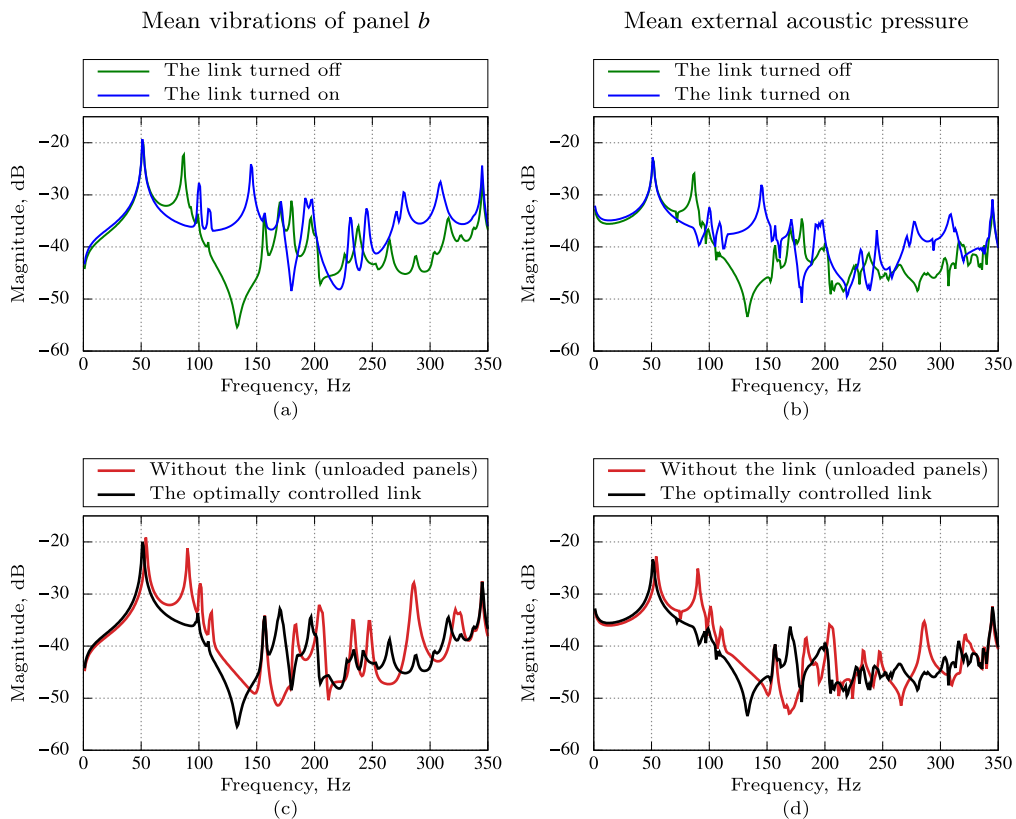
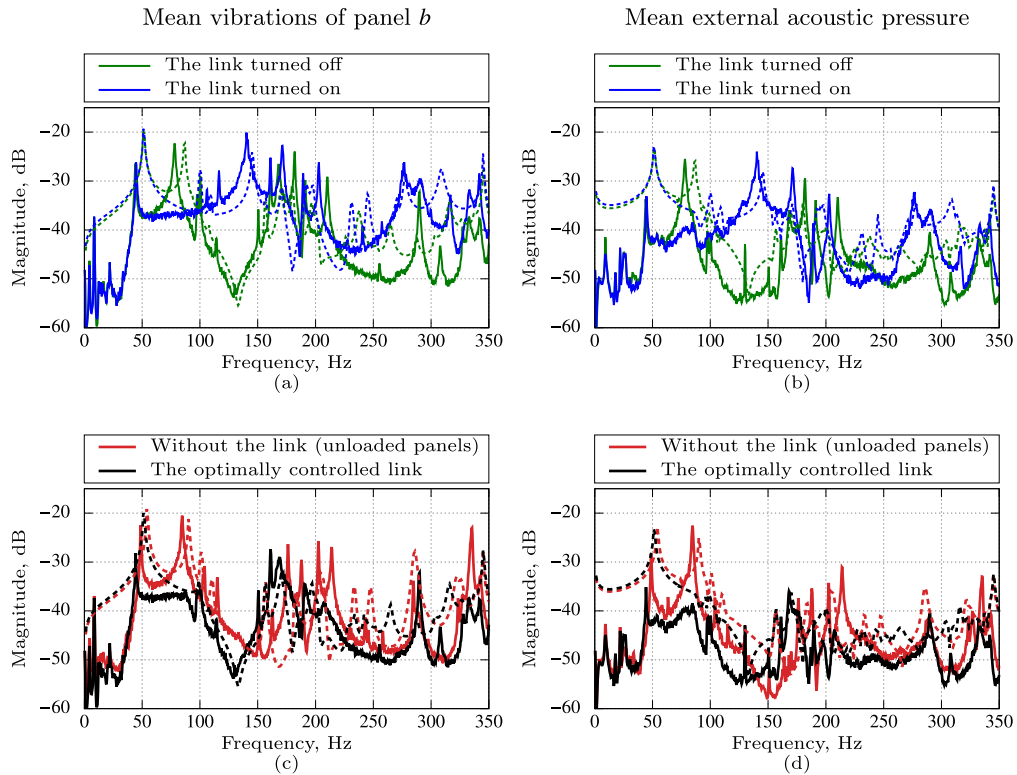


Fig. 6. Frequency characteristics for the semi-active control numerical simulation performed for the link mounted between the panels at  $x_{L,1} = 0.5L_{a,x}$  and  $y_{L,j} = 0.5L_{a,y}$ . Both panels are of the same thickness equal to 1 mm.



**Fig. 7.** Frequency characteristics for the semi-active control numerical simulation presented in Fig. 6 (plotted with dashed lines) overlaid for comparison with experimental results presented in Fig. 5 (plotted with solid lines).

compared to the unloaded double-panel structure (e.g. around 170 Hz). However, the bands with successful noise reduction outweighs them.

#### 4.2. The semi-active link with panels of different thickness

In this simulation, the thickness of panel *a* was increased from 1 mm to 2 mm. The frequency characteristics obtained are presented in Fig. 8. The first important conclusion is that for a double-panel barrier with panels of different thicknesses, the semi-active link is able to change, thus reducing the fundamental frequency, i.e. when both panels vibrate in-phase with mode shape (1,1). The mass-air-mass resonance is mitigated in a similar manner to symmetric panel configuration. The noise transmission in the remaining part of the frequency band being considered remains rather similar to the symmetric configuration. Thus, it shows that asymmetric configuration is substantially more beneficial compared to the symmetric one.

#### 4.3. A link with additional mass

If a symmetric double-panel barrier configuration has to be employed for any reason, e.g. the application of a semi-active control system to an already existing structure, an additional passive mass can be added to one of the panels to alter its natural frequencies and help mitigate the fundamental frequency with the semi-active link. The simulation results obtained for symmetric panels with a passive mass of 0.25 kg attached to panel *b* at its center are given in Fig. 9. Although the asymmetric configuration, whenever possible, still seems to be a better choice, the addition of mass to one of the panels definitely helps in reduction of the fundamental mode; for the case considered, 7 dB more reduction of mean external acoustic pressure can be obtained compared to the case without the additional mass. An alternative could be to attach an additional stiffener to panel *b* as in [31,28], instead of additional mass, in order to alter the fundamental mode frequency of one of the panels.

#### 4.4. Three semi-active links

Finally, a scenario is considered with three semi-active links introduced into the gap cavity. The number of three links was arbitrarily chosen in order to explore the option of increasing the number of semi-active links, while maintaining still reasonable number of them for practical applications. In the example presented, their locations have been arbitrarily chosen, however, a number of arrangements have been simulated to validate the conclusion presented in this subsection. The sim-

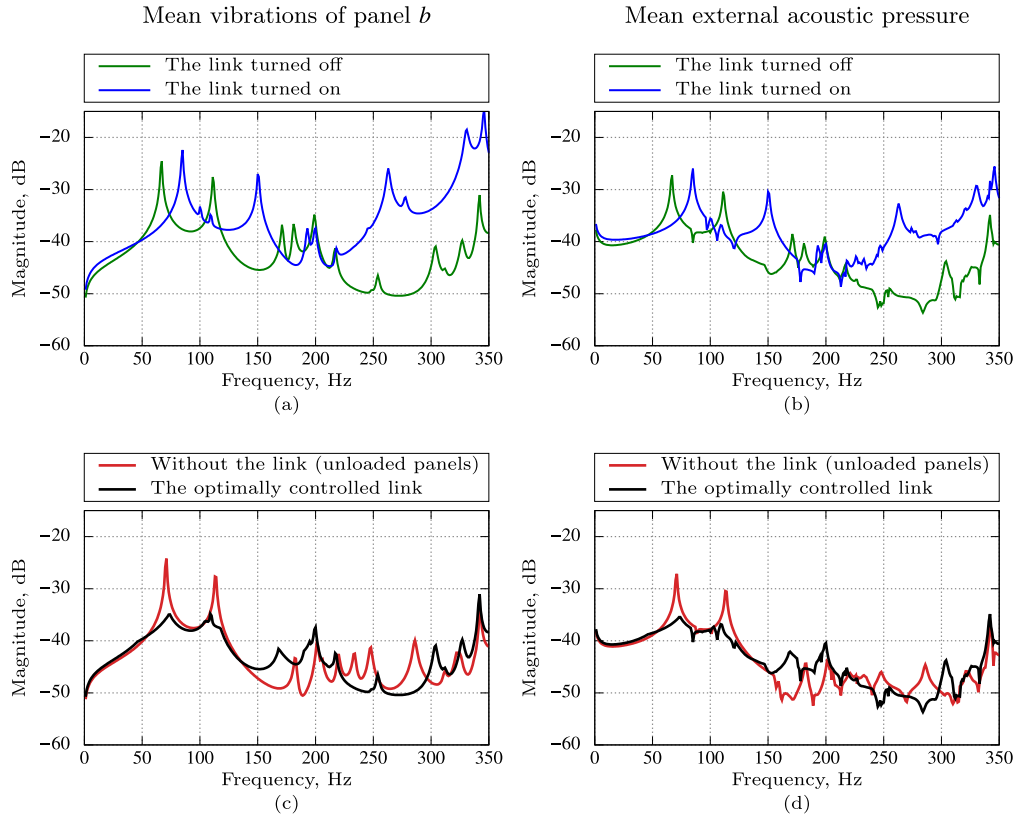


**Fig. 8.** Frequency characteristics for the semi-active control numerical simulation performed for the link mounted between the panels at  $x_{L,1} = 0.5L_{a,x}$  and  $y_{L,1} = 0.5L_{a,y}$ . Panel  $b$  thickness  $h_b = 1$  mm, while panel  $a$  thickness  $h_a = 2$  mm.

ulation results are given in Fig. 10. An asymmetric configuration with  $h_a = 2$  mm and  $h_b = 1$  mm has been used. The links were located at:

$$\begin{aligned} x_{L,1} &= 0.50L_{a,x}, & y_{L,1} &= 0.50L_{a,y}, \\ x_{L,2} &= 0.83L_{a,x}, & y_{L,2} &= 0.50L_{a,y}, \\ x_{L,3} &= 0.25L_{a,x}, & y_{L,3} &= 0.20L_{a,y}. \end{aligned}$$

To determine which links are turned on, a vector  $K_L = [K_{L,1} \ K_{L,2} \ K_{L,3}]$  can be defined, assuming that  $K_{L,i} = 0\text{N/m}$  when the link is turned off, and  $K_{L,i} = 10^6\text{N/m}$  when the link is turned on.

The analysis of Fig. 10 leads to a conclusion that both fundamental and mass-air-mass resonances are successfully mitigated (as for a single link), but above a certain frequency (in the example considered, above 200 Hz), a configuration with all links turned off provides a continuously better performance; turning on any of the links can only worsen the transmission loss. It is due to a phenomenon that for higher frequencies the double-panel barrier itself provides good passive transmission loss, and adding a structural link at any location, although altering frequencies and mode shapes, enhances the overall energy transmission between the panels and generally worsens the transmission loss; a structural energy transmission path, in addition to the acoustic path, is added to the system.

In addition, comparing Figs. 8 and 10 leads to a conclusion, that the improvement due to an increased number of semi-active links is rather weak. A single link located at the center of the panels is effective enough to mitigate low-order resonances (fundamental and mass-air-mass resonances, which are most responsible for weak transmission loss performance of the double-panel barrier). For higher resonances, the links considered are not useful, hence addition of more links is rather unjustified.

#### 4.5. Energy transmission analysis

Through a double-panel barrier, energy can be transmitted either through the acoustic path or through the structural path with a mechanical link. The already observed phenomena determining the performance of the proposed semi-active link can be well understood when analyzing the energy transmission process.

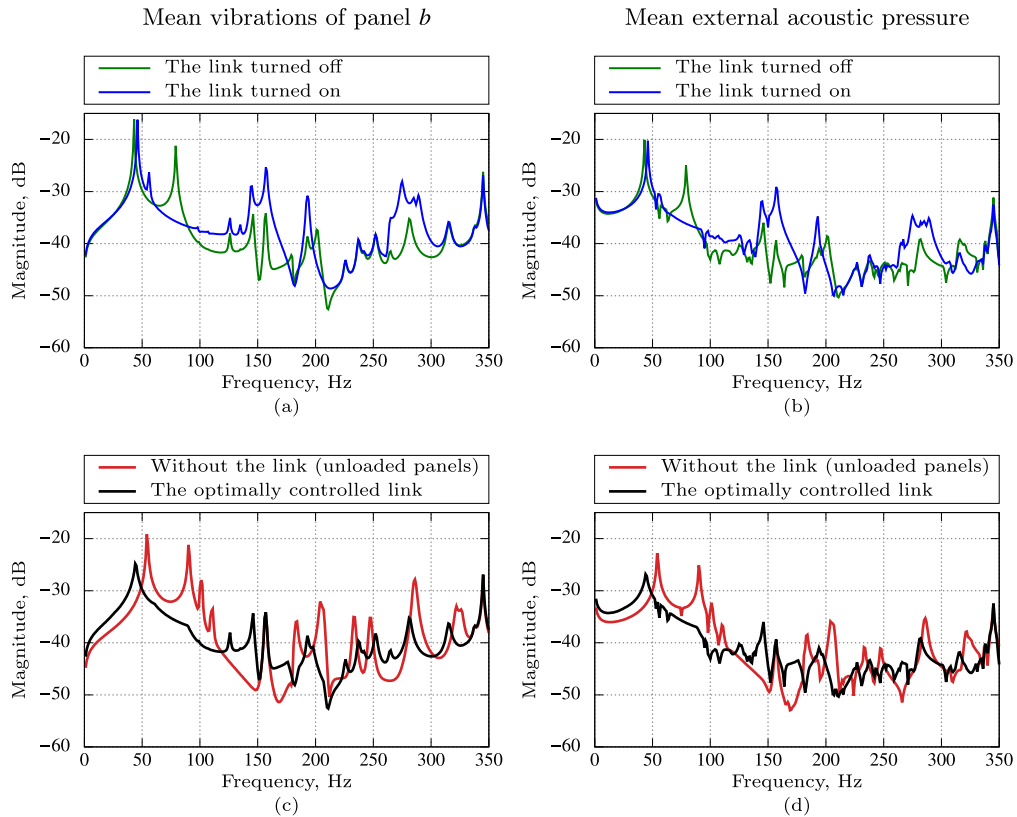


**Fig. 9.** Frequency characteristics for the semi-active control numerical simulation performed for the link mounted between the panels at  $x_{L1} = 0.5L_{ax}$  and  $y_{Lj} = 0.5L_{ay}$ . Both panels are of the same thickness equal to 1 mm, but an additional mass of 0.25 kg is attached to panel  $b$  at its center.

Fig. 11 presents the tendency plot of the mean vibration velocity amplitude of panel  $b$ , averaged over the frequency band between 0 Hz and 350 Hz, in function of gap depth  $L_{g,z}$ . The mean vibration magnitudes are considered as a rough representation of the overall energy transmitted from the noise source to the radiating surface of the barrier within the analyzed frequency band. The plots are presented for the link turned off, the link turned on, and for the optimally controlled semi-active link. Following the observations provided in [25], in Fig. 11 three zones can be distinguished.

For the lowest values of  $L_{g,z}$ , the distance between the panels is so short that the acoustic energy transmission path is dominant, hence switching the link on or off has a very weak impact on the overall energy transmission. It is well illustrated in Fig. 12a, where frequency characteristics for the numerical simulations of the barrier with gap depth  $L_{g,z} = 0.004$  m is presented.

By increasing the gap depth  $L_{g,z}$ , the structural path (when the link is turned on) becomes comparable to the acoustic path. Hence, the addition of the structural path affects substantially the vibrations of panel  $b$ , and the semi-active control can choose a more beneficial configuration (cf. Figs. 12bc). The magnitudes obtained for "the optimally controlled link" in Fig. 11 becomes much better comparing to the link permanently turned on or off.

However, a further increase of the gap depth  $L_{g,z}$  results in the acoustic path becoming weaker than the structural path, especially for the higher frequencies; the tendency plot for the link turned off in Fig. 11 becomes continuously lower, while the plot for the link turned on already reached a plateau. Hence, for nearly all frequencies it is better to keep the link turned off, taking advantage of the transmission loss provided the double-panel structure itself (cf. Fig. 12d).

The provided analysis gives hints on the choice of the gap depth  $L_{g,z}$  when designing a semi-active double-panel barrier (there is clearly an optimal range of values). But more importantly, it provides an insight and explains the physical phenomena behind the performance of the proposed semi-active links.

## 5. Conclusions

Novel noise control methods are being sought in the increasingly noise-polluted world, and are especially attractive if they can be energy-efficient. This paper proposes an original semi-active control approach for double-panel noise barriers that mitigates low-order resonances which are most responsible for weak transmission loss performance of double-panel noise barriers.

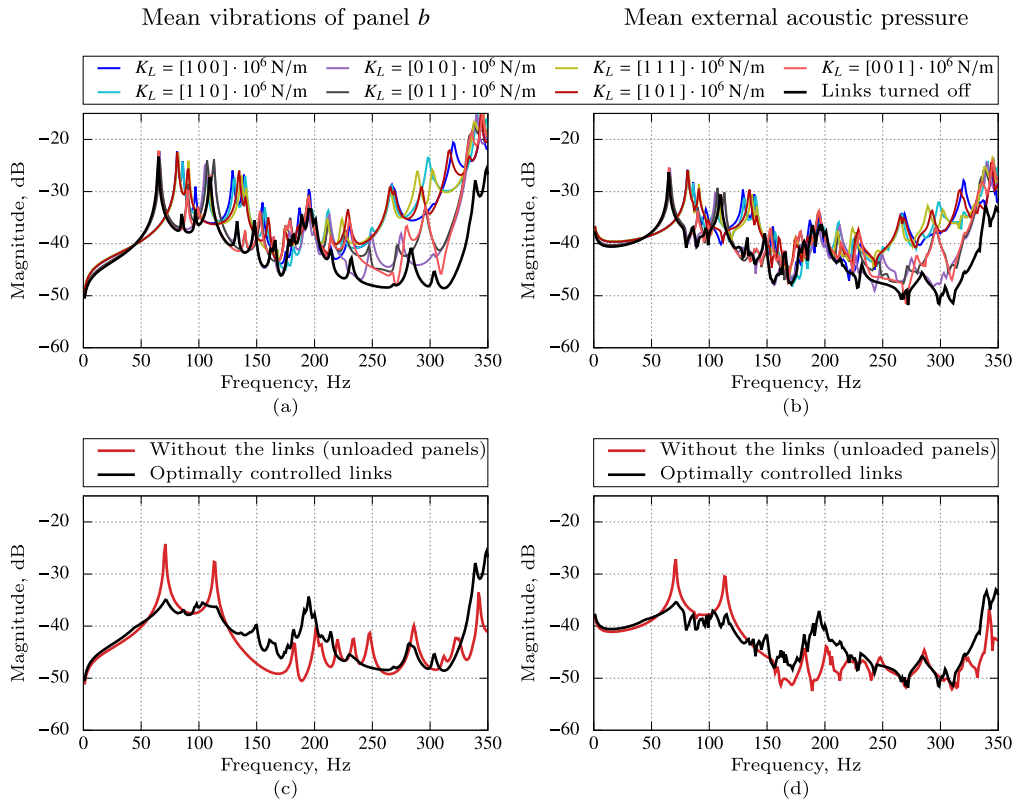


**Fig. 10.** Frequency characteristics for the semi-active control numerical simulation performed for three links mounted between the panels. Panel *b* thickness  $h_b = 1$  mm, while panel *a* thickness  $h_a = 2$  mm.

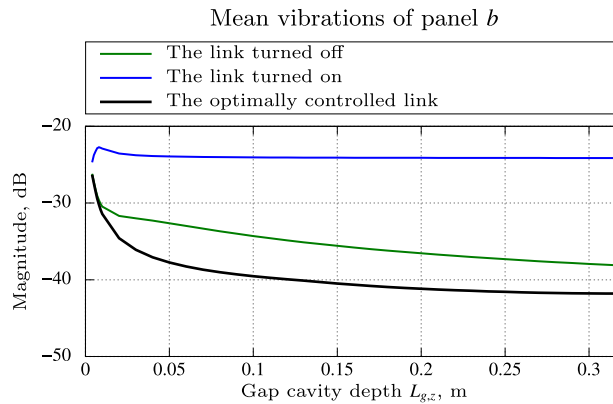


**Fig. 11.** Tendency plot of the mean vibrations of panel *b*, averaged over the frequency band between 0 Hz and 350 Hz, in function of gap depth  $L_{g,z}$ . The numerical simulations were performed for the semi-active link mounted between the panels at  $x_{L,1} = 0.5L_{ax}$  and  $y_{L,j} = 0.5L_{ay}$ . Panel *b* thickness  $h_b = 1$  mm, while panel *a* thickness  $h_a = 2$  mm.

A mathematical model of the double-panel barrier, including semi-active links, loading due to their mass, and adjacent enclosure for the noise source has been derived. Both the model and the semi-active control approach have been experimentally validated. Then, numerical simulation studies have been performed to provide analysis and insight into various practical aspects. The analysis of the energy transmission process is provided.

Summarizing the main conclusions, a single semi-active link located at the center of both panels can successfully mitigate low-order resonances reducing the acoustic radiation of the barrier for narrow-band noise even by 16 dB. The external energy is only needed to switch states of the link. Moreover, there is clearly an optimal range of gap cavity depth  $L_{g,z}$ , when

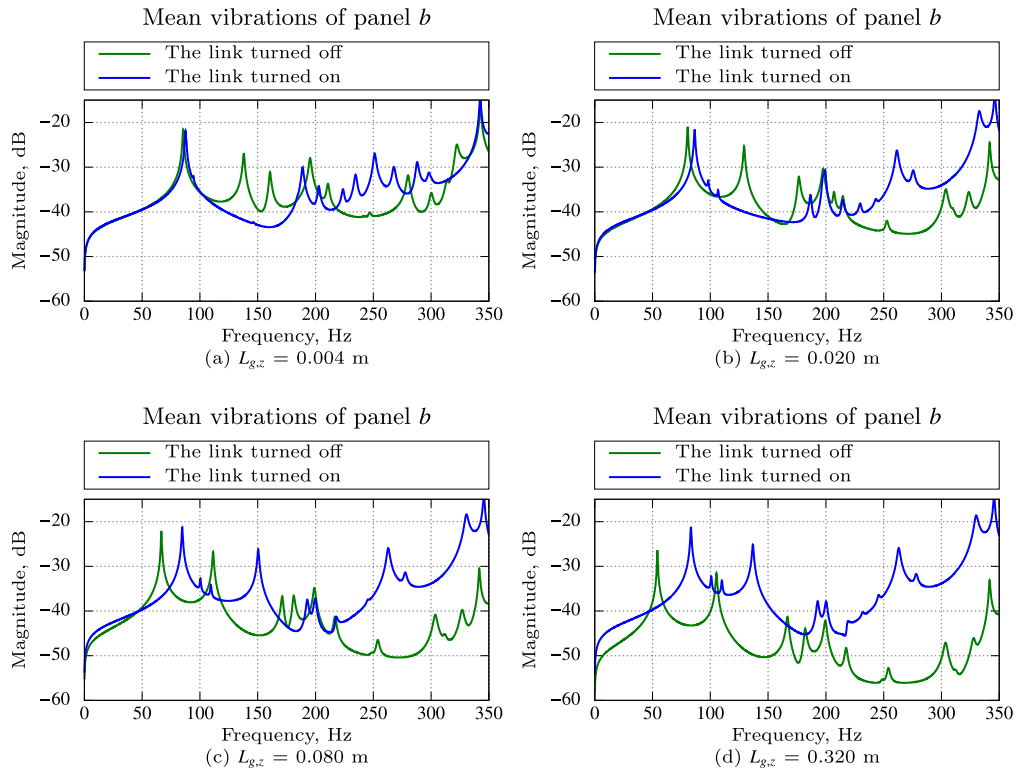


**Fig. 12.** Frequency characteristics for the numerical simulations of the barrier with different gap depth  $L_{g,z}$ . The simulations were performed for the semi-active link mounted between the panels at  $x_{L,1} = 0.5L_{a,x}$  and  $y_{L,j} = 0.5L_{a,y}$ . Panel  $b$  thickness  $h_b = 1$  mm, while panel  $a$  thickness  $h_a = 2$  mm.

both acoustic and structural energy transmission paths are comparable, allowing the semi-active links to reach its best performance.

More links and different arrangements seem to be ineffective for improving higher frequency insulation due to physical phenomena occurring in double-panel structures. Nevertheless, the proposed semi-active link can be used jointly with other types of semi-active actuators that do not couple panels structurally, preserving the good transmission loss for higher frequencies provided by the structure itself. Such alternative actuators could semi-actively adapt stiffness or mass distribution of a panel. The semi-active link would then be responsible for the low-order resonances, while other semi-active actuators would alter higher resonances. Such combined technique would further develop the proposed semi-active approach.

### CRedit authorship contribution statement

**Stanislaw Wrona:** Conceptualization, Methodology, Software, Validation, Formal analysis, Investigation, Resources, Data curation, Writing - original draft, Writing - review & editing. **Marek Pawelczyk:** Conceptualization, Validation, Writing - original draft, Writing - review & editing, Supervision, Project administration, Funding acquisition. **Li Cheng:** Conceptualization, Validation, Formal analysis, Writing - review & editing.

### Declaration of Competing Interest

The authors declare that they have no known competing financial interests or personal relationships that could have appeared to influence the work reported in this paper.

### Acknowledgment

The authors are indebted to anonymous reviewers for their precious comments and suggestions, which helped improving the paper.

The research reported in this paper has been supported by the National Science Centre, Poland, decision No. DEC-2017/25/B/ST7/02236.

**Appendix A**

$$H_{11} = \left[ \text{diag}(m_{a,i}(\omega_{a,i}^2 + 21\zeta_{a,i}\omega_{a,i}\omega - \omega^2)) \right] + \sum_{j=1}^{N_i} K_{Lj} \psi_a^T(x_{Lj}, y_{Lj}) \psi_a(x_{Lj}, y_{Lj}),$$

$$H_{22} = \left[ \text{diag}(m_{b,i}(\omega_{b,i}^2 + 21\zeta_{b,i}\omega_{b,i}\omega - \omega^2)) \right] + \sum_{j=1}^{N_i} K_{Lj} \psi_b^T(x_{Lj}, y_{Lj}) \psi_b(x_{Lj}, y_{Lj}),$$

$$H_{33} = \left[ \text{diag}(\omega_{e,i}^2 + 21\zeta_{e,i}\omega_{e,i}\omega - \omega^2) \right],$$

$$H_{44} = \left[ \text{diag}(\omega_{g,i}^2 + 21\zeta_{g,i}\omega_{g,i}\omega - \omega^2) \right],$$

$$H_{12} = - \sum_{j=1}^{N_i} K_{Lj} \psi_a^T(x_{Lj}, y_{Lj}) \psi_b(x_{Lj}, y_{Lj}),$$

$$H_{21} = H_{12}^T,$$

$$H_{13} = -S_a \begin{bmatrix} L_{ae,11} & \dots & L_{ae,1N_e} \\ \vdots & \ddots & \vdots \\ L_{ae,N_a1} & \dots & L_{ae,N_aN_e} \end{bmatrix},$$

$$H_{14} = S_a \begin{bmatrix} L_{ag,11} & \dots & L_{ag,1N_g} \\ \vdots & \ddots & \vdots \\ L_{ag,N_a1} & \dots & L_{ag,N_aN_g} \end{bmatrix},$$

$$H_{24} = -S_b \begin{bmatrix} L_{bg,11} & \dots & L_{bg,1N_g} \\ \vdots & \ddots & \vdots \\ L_{bg,N_b1} & \dots & L_{bg,N_bN_g} \end{bmatrix},$$

$$H_{31} = - \frac{\rho_p c_p^2 S_a \omega^2}{V_e} \begin{bmatrix} \frac{1}{m_{e,1}} L_{ae,11} & \dots & \frac{1}{m_{e,1}} L_{ae,N_a1} \\ \vdots & \ddots & \vdots \\ \frac{1}{m_{e,N_e}} L_{ae,1N_e} & \dots & \frac{1}{m_{e,N_e}} L_{ae,N_aN_e} \end{bmatrix},$$

$$H_{41} = \frac{\rho_p c_p^2 S_a \omega^2}{V_g} \begin{bmatrix} \frac{1}{m_{g,1}} L_{ag,11} & \dots & \frac{1}{m_{g,1}} L_{ag,N_a1} \\ \vdots & \ddots & \vdots \\ \frac{1}{m_{g,N_g}} L_{ag,1N_g} & \dots & \frac{1}{m_{g,N_g}} L_{ag,N_aN_g} \end{bmatrix},$$

$$H_{42} = - \frac{\rho_p c_p^2 S_b \omega^2}{V_g} \begin{bmatrix} \frac{1}{m_{g,1}} L_{bg,11} & \dots & \frac{1}{m_{g,1}} L_{bg,N_b1} \\ \vdots & \ddots & \vdots \\ \frac{1}{m_{g,N_g}} L_{bg,1N_g} & \dots & \frac{1}{m_{g,N_g}} L_{bg,N_bN_g} \end{bmatrix},$$

**References**

- [1] J. Milton, J. Cheer, S. Daley, Active structural acoustic control using an experimentally identified radiation resistance matrix, *J. Acoust. Soc. Am.* 147 (3) (2020) 1459–1468.
- [2] S. Wrona, M. Pawelczyk, Active reduction of device narrowband noise by controlling vibration of its casing based on structural sensors, in: Proceedings of 22nd International Congress on Sound and Vibration, Florence, Italy, 12–16 July, 2015.
- [3] K. Mazur, S. Wrona, M. Pawelczyk, Active noise control for a washing machine, *Appl. Acoust.* 146 (2019) 89–95.
- [4] Y. Li, L. Cheng, Mechanisms of active control of sound transmission through a linked double-wall system into an acoustic cavity, *Appl. Acoust.* 69 (7) (2008) 614–623.
- [5] X. Qiu, *An Introduction to Virtual Sound Barriers*, CRC Press, 2019.
- [6] D. Shi, W.-S. Gan, B. Lam, R. Hasegawa, Y. Kajikawa, Feedforward multichannel virtual-sensing active control of noise through an aperture: Analysis on causality and sensor-actuator constraints, *J. Acoust. Soc. Am.* 147 (1) (2020) 32–48.
- [7] Q. Mao, S. Pietrzko, *Control of Noise and Structural Vibration*, Springer, 2013.
- [8] O. Kaiser, S. Pietrzko, M. Morari, Feedback control of sound transmission through a double glazed window, *J. Sound Vib.* 263 (4) (2003) 775–795.
- [9] W. Zheng, Y. Lei, Q. Huang, S. Li, Improving low frequency performance of double-wall structure using piezoelectric transducer/loudspeaker shunt damping technologies, *J. Low Frequency Noise Vib. Active Control* 31 (3) (2012) 175–192.
- [10] F. Langfeldt, H. Hoppen, W. Gleine, Broadband low-frequency sound transmission loss improvement of double walls with helmholtz resonators, *J. Sound Vib.* (2020) 115309.
- [11] N. de Melo Filho, L. Van Belle, C. Claeys, E. Deckers, W. Desmet, Dynamic mass based sound transmission loss prediction of vibro-acoustic metamaterial double panels applied to the mass-air-mass resonance, *J. Sound Vib.* 442 (2019) 28–44.

- [12] Q. Mao, Improvement on sound transmission loss through a double-plate structure by using electromagnetic shunt damper, *Appl. Acoust.* 158 (2020) 107075.
- [13] X. Ma, K. Chen, J. Xu, Active control of sound transmission through orthogonally rib stiffened double-panel structure: Mechanism analysis, *Appl. Sci.* 9 (16) (2019) 3286.
- [14] E. Turco, P. Gardonio, Sweeping shunted electro-magnetic tuneable vibration absorber: Design and implementation, *J. Sound Vib.* 407 (2017) 82–105.
- [15] P. Gardonio, M. Zientek, L. Dal Bo, Panel with self-tuning shunted piezoelectric patches for broadband flexural vibration control, *Mech. Syst. Signal Process.* 134 (2019) 106299.
- [16] K. Billon, N. Montcoudiol, A. Aubry, R. Pascual, F. Mosca, F. Jean, C. Pezerat, C. Bricault, S. Chesné, Vibration isolation and damping using a piezoelectric flextensional suspension with a negative capacitance shunt, *Mech. Syst. Signal Process.* 140 (2020) 106696.
- [17] L. Dal Bo, P. Gardonio, D. Casagrande, S. Saggini, Smart panel with sweeping and switching piezoelectric patch vibration absorbers: Experimental results, *Mech. Syst. Signal Process.* 120 (2019) 308–325.
- [18] Q. Mao, S. Pietrzko, Experimental study for control of sound transmission through double glazed window using optimally tuned helmholtz resonators, *Appl. Acoust.* 71 (1) (2010) 32–38.
- [19] H. Lissek, R. Boulandet, R. Fleury, Electroacoustic absorbers: bridging the gap between shunt loudspeakers and active sound absorption, *J. Acoust. Soc. Am.* 129 (5) (2011) 2968–2978.
- [20] S.S. Rao. *Vibration of continuous systems*, vol. 464, Wiley Online Library, 2007.
- [21] D. Young, Vibration of rectangular plates by the ritz method, *J. Appl. Mech. Trans. ASME* 17 (4) (1950) 448–453.
- [22] K. Kim, B.-H. Kim, T.-M. Choi, D.-S. Cho, Free vibration analysis of rectangular plate with arbitrary edge constraints using characteristic orthogonal polynomials in assumed mode method, *Int. J. Naval Archit. Ocean Eng.* 4 (3) (2012) 267–280.
- [23] R.R. Craig, A.J. Kurdila, *Fundamentals of structural dynamics*, John Wiley & Sons, 2006.
- [24] I.L. Ver, L.L. Beranek, *Noise and Vibration Control Engineering-Principles and Applications*, Wiley, 2006: *Noise and Vibration Control Engineering-Principles and Applications*, John Wiley & Sons Inc, 2006.
- [25] L. Cheng, Y. Li, J. Gao, Energy transmission in a mechanically-linked double-wall structure coupled to an acoustic enclosure, *J. Acoust. Soc. Am.* 117 (5) (2005) 2742–2751.
- [26] W. Rdzanek, *Structural vibroacoustics of surface elements* [in Polish: *Wibroakustyka strukturalna elementów powierzchniowych*], Rzeszów University of Technology Publishing House, 2011.
- [27] E. Skudrzyk, *The foundations of acoustics: basic mathematics and basic acoustics*, Springer Science & Business Media, 2012.
- [28] S. Wrona, M. Pawelczyk, X. Qiu, Shaping the acoustic radiation of a vibrating plate, *J. Sound Vib.* (2020) 115285.
- [29] J. Bakker, D.M. Frangopol, K. van Breugel, *Life-Cycle of Engineering Systems: Emphasis on Sustainable Civil Infrastructure: Proceedings of the Fifth International Symposium on Life-Cycle Civil Engineering*, CRC Press, Delft, The Netherlands, 2016.
- [30] N. de Melo Filho, C. Claeys, E. Deckers, W. Desmet, Metamaterial foam core sandwich panel designed to attenuate the mass-spring-mass resonance sound transmission loss dip, *Mechanical Systems and Signal Processing* 139 (2020) 106624.
- [31] S. Wrona, M. Pawelczyk, Shaping frequency response of a vibrating plate for passive and active control applications by simultaneous optimization of arrangement of additional masses and ribs. Part I: Modeling, *Mech. Syst. Signal Process.* 70–71 (2016) 682–698.